Deciphering Molecular Self-Assembly through Electron Microscopy and Fluorescence Correlation Spectroscopy

Subhankar Kundu, Arkaprava Chowdhury, Somen Nandi, Kankan Bhattacharyya,* Abhijit Patra*

KEYWORDS. Molecular self-assembly, morphological evolution, nanofiber, fluorescence correlation spectroscopy, thiophene derivative.

ABSTRACT: Supramolecular self-assembly of small organic molecules has emerged as a powerful tool to construct well-defined micro- and nanoarchitecture through fine-tuning a range of intermolecular interactions. The size, shape, and optical properties of these nanostructures largely depend on the temperature and polarity of the medium, along with the specific self-assembled pattern of molecular building units. The engineering of supramolecular self-assembled nanostructures with morphology-dependent tunable emission is in high demand due to the promising scope in nanodevices and molecular machines. However, challenges are probing the evolution of molecular aggregates from a true solution and directing the self-assembly process in a pre-defined fashion. The structure of molecular aggregates in the solution can be predicted from fluorescence correlation spectroscopy (FCS) and dynamic light scattering (DLS) analysis. On the other hand, the morphology of the aggregates can also be visualized through electron microscopy. Nevertheless, a direct correlation between emission from molecular aggregates in the aqueous dispersion and their morphology obtained through a solid-state characterization is missing. In the present study, we decipher the sequential evolution of molecular nanofibers from solution to spherical and oblong-shaped nanoparticles through the variation of solvent polarity, adjusting the hydrophobic-hydrophilic interactions. The intriguing case of molecular self-assembly is elucidated employing a newly designed π-conjugated thiophene derivative (TPAn) through a combination of steady-state absorption, emission measurements, FCS, and electron microscopy. The FCS analysis and microscopy results infer that small-sized nanofibers in the dispersion are further agglomerated, resulting in a network of nanofibers upon solvent evaporation. The evolution of organic nanofibers and subtle control over the self-assembly process demonstrated in the current investigation provides a general paradigm to correlate the size, shape, and emission properties of diverse fluorescent molecular aggregates in complex heterogeneous media, including a human cell.

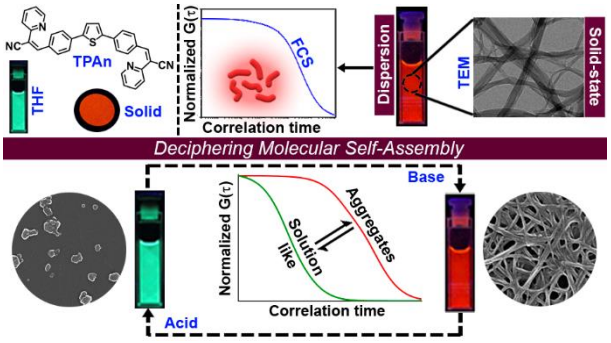

INTRODUCTION

'Self-assembly' plays a crucial role in the formation of diverse, complex biological structures from single molecular building units.[1-3] In living systems, the self-assembly arises from hydrophilic and hydrophobic interactions.[4-6] The hydrophilic interactions involve direct hydrogen bonds or electrostatic interactions between biomolecules and water.[7] The hydrophobic interactions refer to the tendency of self-aggregation of apolar moieties of biomolecules in aqueous solution through the minimal disruption of water-water hydrogen bonds.[5, 8-11] As for the example, the double-helical filaments (F-actin) are formed through spontaneous self-assembly of globular actin (G-actin).[12, 13] The double helix structure of DNA moulds via the zipping up of the two long chains of nucleotides connected through hydrogen bonds between the complementary base pairs.[14] Inspired by the natural self-assembly processes, researchers have been constructing artificial supramolecular assemblies.[2, 6, 15-28] The supramolecular self-association of small π-conjugated organic molecules leads to well-defined nanoarchitectures like vesicles, micelles, low molecular weight gels, and noncovalent aggregates of diverse shape through a range of intermolecular interactions.[17, 29-36] Such molecular aggregates found applications ranging from light-harvesting, biomedicine, bioimaging to sensors and switches.[37-42] Interestingly, the emission property and biological activity of self-assembled molecular aggregates largely depend on their morphology.[36, 43-46]

Recently, the morphology-dependent spectral properties of organic aggregates have been rationalized through various analytical approaches.[44, 46] Würthner and coworkers studied the morphology-dependent tunable emission for amphiphilic perylene bisimide nanoaggregates through a combined transmission electron microscopy (TEM) and steady-state absorption and emission analysis.[44] Matsuda and coworkers studied the reversible morphological transformation of supramolecular assembly of amphiphilic diarylethene between microspheres and fibers through polarized optical microscopy (POM), TEM, and X-ray diffraction (XRD).[46] In many cases, the self-assembled structures have emerged from a competition of intermolecular interactions between organic solutes among themselves and with solvents.[47-50] Thus, the correlation between the morphological evolution (through a solid-state characterization) and the emission behaviour (dispersion-state analysis) of the molecular aggregates is often rudimentary and can be benefitted through further analysis. Fluorescence correlation spectroscopy (FCS) and dynamic light scattering (DLS) analysis are used to investigate structures in solutions.[51, 52] Of late, Ganguli and coworkers demonstrated the growth mechanism of iron oxalate nanorods from nanoparticles through fluorescence correlation spectroscopy (FCS), dynamic light scattering (DLS), and transmission electron microscopy (TEM).[51]

Herein, we presented a unified picture on the evolution of all-organic nanofibers from solution through spherical nanoaggregates by a combined spectroscopic and microscopic approach using steady-state absorption, emission, and FCS analysis coupled with field-emission scanning electron microscopy (FESEM) and TEM (Figure 1). We developed a new thiophene-based acceptor-π-donor-π-acceptor (A-π-D-π-A) fluorescent probe (TPAn) to understand the molecular self-assembly toward the formation of the anisotropic nanostructure. The polarity of the dispersion medium was adjusted to obtain the anisotropic nanofibers from spherical nanoparticles through tuning the hydrophobic-hydrophilic interactions. We elucidated the role of pyridinic nitrogen centers in TPAn governing the self-assembly through the stimuli-responsive reversible morphological transformation from the nanofibers to nanoparticles. Molecular modeling studies shed light on the formation of intermolecular interactions-driven three-dimensional (3D) supramolecular assembly. The effect of microenvironments on physicochemical properties of TPAn was probed in a complex, heterogeneous medium, like human cells comparing with that in the bulk solution and self-assembled molecular aggregates.

RESULTS AND DISCUSSION

The design strategy of TPAn involved the electron acceptor (2-pyridoacetonitrile) units, as the two arms, attached to the central thiophene ring through phenyl spacers (Figure 1). The donor-acceptor molecule displayed tunable emission with varying solvent polarity. The incorporation of phenyl spacers allowed an extended π-electron conjugation as well as the angular geometry. The geometry optimization inferred that such molecular architecture would prevent the π-π stacking leading to strong fluorescence in the aggregated as well as solid-state.

In a typical synthetic protocol, TPAn was synthesized through the metal-free Knoevenagel condensation reaction between 4,4'-(thiophene-2,5-diyl)dibenzaldehyde (TBA) and 2-pyridylacetonitrile (Figure 1). Both TBA and TPAn were characterized by ^{1}H NMR, ^{13}C NMR spectroscopy, and mass spectrometry. The broad absorption band of TPAn at 320 to 470 nm in solvents of varying polarity was due to the extended π-conjugation from the donor thiophene core to electron-withdrawing pyridylacetonitrile units. The emission spectra of TPAn in nonpolar (toluene) to intermediate polar [tetrahydrofuran (THF), and chloroform] solvents revealed multiple feature bands. However, a broad, red-shifted emission band was observed due to the facile intramolecular charge-transfer (ICT) in the excited state in polar solvents like *N, N* dimethylformamide, and dimethyl sulfoxide (DMSO).

Aggregation behaviour. Self-assembly of TPAn was probed employing water, inducing molecular aggregation, as customary for hydrophobic molecules. Theoretical studies and molecular simulations suggested the rupture of hydrogen bonds of water to accommodate nonpolar organic molecules (hydrophobe).[9, 11, 53] The loss of hydrogen bonding architecture results in fluctuation and depletion of water density near the nonpolar solutes causing them to collapse.[53] In addition to the chemical structure of the

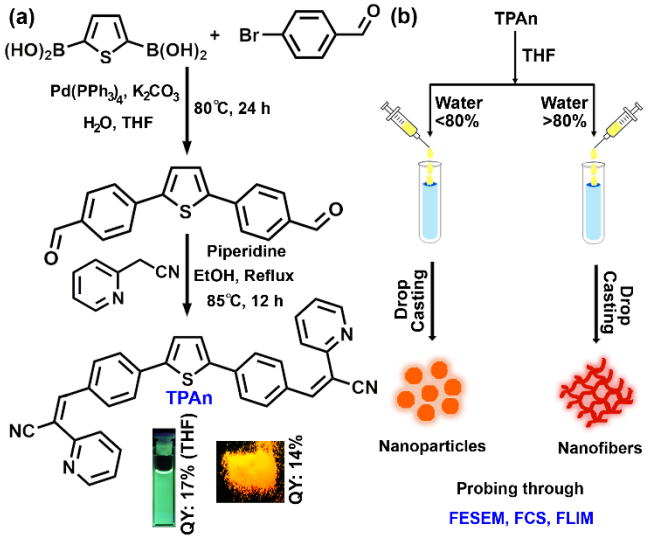

Figure 1. (a) Synthetic route for TPAn involving Suzuki coupling between thiophene-2,5-diyldiboronic acid and 4-bromobenzaldehyde, followed by Knoevenagel condensation between C-C coupled product, 4,4'-(thiophene-2,5-diyl)dibenzaldehyde and 2-pyridylacetonitrile. The digital photographs demonstrating strong emission of TPAn in solution and powder under the illumination at 365 nm; respective fluorescence quantum yields (QY) are mentioned. (b) Schematic illustration depicting the formation of TPAn nanoparticles and nanofibers with varying the composition of the THF-water mixture probed through a combined microscopic and spectroscopic approach.

hydrophobe, the shape and size of molecular aggregates can also be tuned through the variation of the environmental conditions like light, temperature, and polarity of the medium.[46-48, 54-56] In the present work, we demonstrated the impact of the polarity of solvents on the dynamic morphological transformation of TPAn aggregates. The aggregation behavior of TPAn was investigated in a binary solvent mixture of tetrahydrofuran (good solvent) and water (bad solvent) with varying the fraction of water from 0% to 90%. An abrupt change in both the absorption and emission was observed at 80% water fraction (Figure 2a and 2b). A blue-shift in the absorption and a large red-shift in the emission similar to that observed in the powder form (Figure 2a and 2b) with diminished fluorescence was presumably due to the formation of molecular aggregates. The plot of the extent of aggregation against the fraction of water revealed the steep rise at 70-80% water fraction, indicating it as the most significant regime of aggregation of TPAn (Figure 2c).

Electron microscopy. The morphology of the self-assembled aggregates was monitored through FESEM and TEM. The samples were prepared by drop-casting of TPAn dispersions. A drastic morphological transformation from nanoparticles to nanofibers was observed for the samples with increasing water fraction (Figure 2d-g). Spherical to oblong-shaped nanoparticles to 1D-nanofibers were observed respectively at 60, 70, and 80% water fraction. However, the FESEM images were obtained from the drop-casted samples (solid-state characterization), and the spectroscopic measurements were carried out in the

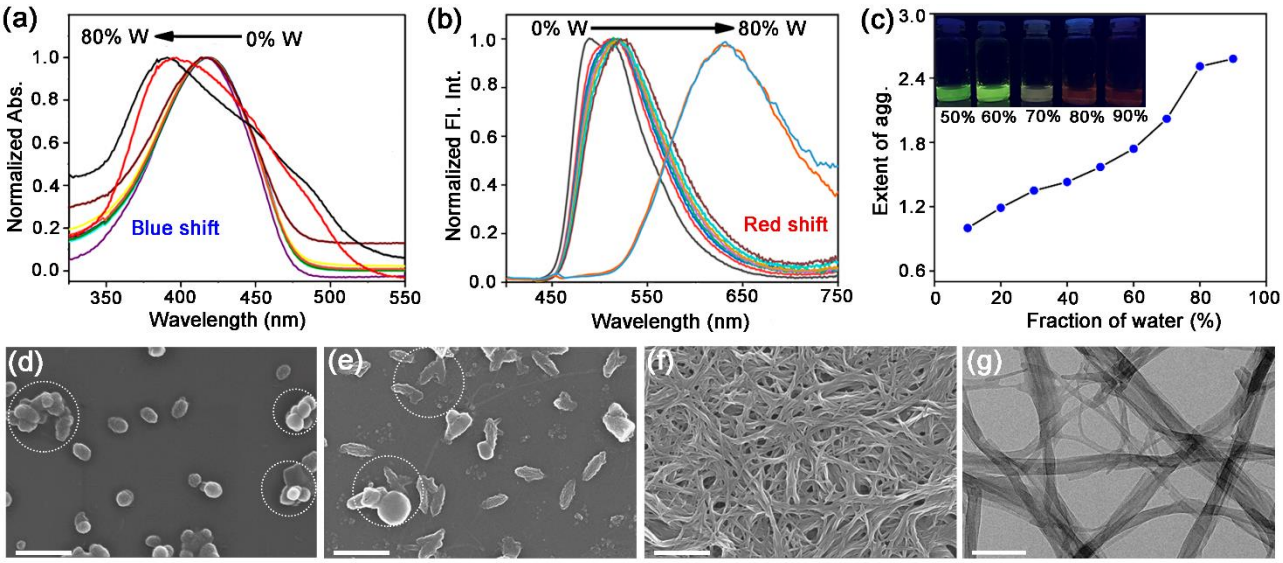

Figure 2. Normalized (a) absorption and (b) emission spectra (excited at individual λ_{abs}) of TPAn (0.2 mM, 30 μL) in 3 mL THF-water mixture with varying the water fraction from 0 to 90% with 10% of interval. (c) The plot of the extent of aggregation against the fraction of water depicting self-assembly of TPAn induced by increasing content of 'bad solvent', water. Inset: the digital photographs of aqueous dispersions of TPAn under the UV light irradiation (λ_{ex} = 365 nm). (d-f) The FESEM images of TPAn in THF-water mixture: (d) 60%, (e) 70%, and (f) 80% water content illustrating aggregation of spherical nanoparticles (60% W), semi-spherical oblong-shaped nanoparticles (70% W) to 1D-nanofibers (80% W). (g) HRTEM image of TPAn aggregates having 80% content of water fraction. Scale (Figure d-g) = 200 nm.

dispersion-state (ensemble measurement). Hence, establishing a direct correlation between the morphology and the emission behavior of TPAn aggregates was quite challenging. The possibility of morphological transformation of TPAn during the preparation of the FESEM, TEM, or atomic force microscopy (AFM) samples due to the solvent evaporation also could not be ignored. Thus, the key question was to establish the self-assembly process toward the formation of nanoparticles to a network of nanofibers with increasing water fraction. It might form in the dispersion-state itself, or there could be an influence of aggregation due to the solvent evaporation during the preparation of samples for electron microscopy.[57-59] Hence, it was worthwhile to comprehend the nature of self-assembly of TPAn in the dispersion-state.

FCS analysis. Nature of the self-assembly in the solid-state and the dispersion can be compared using different analytical tools.[44, 46, 51, 60, 61] As for example, Udgaonkar and coworkers demonstrated the structural evolution of amyloid fibril using atomic force microscopy (AFM) coupled with DLS analysis.[61] Nair and coworkers demonstrated the growth of nanotubes through a combination of DLS, vibrational spectroscopy, and electron microscopy.[60] Instead of ensemble measurements, hydrodynamic radius and length of fluorescent molecules and molecular aggregates can be obtained using FCS.[62] Recently, the growth kinetics, size, and shape of nanostructures, protein aggregates, and micelles in the dispersion-state and dynamics of biological membranes were demonstrated through monitoring the diffusion time and diffusion coefficient of the fluorescent aggregates through FCS.[51, 52, 63, 64] We unravelled the evolution of nanofibers from the true solution through intermediate nanoparticles employing FCS coupled with electron microscopy. We focused on the translational diffusion of TPAn in true solution (THF) and in the form of molecular aggregates (THF-water mixture; Figure 3). Figures 3a and 3b show the normalized autocorrelation curves of TPAn in THF and THF-water mixture with varying water fractions. An apparent discontinuity was observed in the normalized FCS traces for the samples having the water fraction 50-70% (Figure 3b). It was presumably due to the presence of both free and aggregated TPAn molecules. Hence, the fitting of the correlation functions for the samples with 50-70% water fraction was carried out with the two-component diffusion model (equation 1). However, no discontinuity was observed on FCS traces at 80% water fraction. Further, the sample was filtered through a nanoporous Whatman disc (Anodisc, pore size 0.02 μm). The steady-state absorption, emission measurements of the filtrate revealed no signature of free TPAn molecules at 80% water fraction. Hence, the fitting of the FCS traces of TPAn in THF and THF-water mixture with 80% water was carried out using the three-dimensional (3D) diffusion model (equation 2).[65]

$$G(\tau) = \frac{1}{N}\left[\left[\frac{1-y}{\left(1+\frac{\tau}{\tau_{D1}}\right)}\frac{1}{\sqrt{1+\frac{\tau}{\omega^2\tau_{D1}}}}\right] + \left[\frac{y}{\left(1+\frac{\tau}{\tau_{D2}}\right)}\cdot\frac{1}{\sqrt{1+\frac{\tau}{\omega^2\tau_{D2}}}}\right]\right] \quad \text{.....(1)}$$

$$G_{3D}(\tau) = \frac{1}{N}\frac{1}{1+\frac{\tau}{\tau_D}}\frac{1}{\sqrt{1+\frac{\tau}{\omega^2\tau_D}}} \quad \text{.....(2)}$$

Where, $G(\tau)$ is the autocorrelation function, N is the average number of fluorescent particles in the detection volume. ω is the structural parameter of the 3D Gaussian confocal volume, defined as $\omega = \omega_z/\omega_{xy}$, where ω_z is the longitudinal radius, and ω_{xy} is the transverse radius of the focal volume. τ_D is the diffusion time, τ is the correlation time, τ_{D1} and τ_{D2} are the diffusion time of free and

aggregated TPAn molecules, respectively. y refers to the fraction of aggregated TPAn molecules.

The diffusion time (τ_D) and total diffusion constant (D_t) of TPAn (1 nM) in THF was found to be 0.1 ms and 194 μm²/s, respectively. However, significantly slower diffusion (D_t = 1.83 μm²/s) was observed due to the formation of the semi-spherical, oblong-shaped nanoparticles for the sample having 70% of water fraction. Interestingly, the further decrease of the D_t value from 1.7 to 0.57 μm²/s was noticed upon increasing the water fraction from 70 to 80%. The almost 4-fold decrease in the D_t value suggested the formation of nanoaggregates having approximately 4-times larger hydrodynamic radius at 80% water fraction compared to that of 70%. However, FESEM images revealed an abrupt change from semi-spherical, oblong-shaped nanoparticles (70%, Figure 2e) to a network of nanofibers (80%, Figure 2f). The apparent inconsistencies in the observations from FESEM and FCS results indicated the possibility of the presence of smaller anisotropic nanofibers in the dispersion of 80% water fraction. Interestingly, a similar kind of nanofibers network was observed in the HRTEM image for the sample having a 99% water fraction. However, we were unable to get reasonable signals from the FCS measurement that could be fitted. The immobilization of entangled nanofibers (network) in the dispersion with high water content could be the reason. Thus, FCS analysis, coupled with electron microscopy results, implied the formation of a network of nanofibers in the dispersion having a higher percentage of water.

The diameter of the spherical nanoparticles can be calculated using the Stokes-Einstein equation (equation 3).[51] Where, R_h is the hydrodynamic radius of the nanoparticles, k_B is Boltzmann's constant, T is the temperature (20°C in the present case), η is the viscosity of the solvent, and D_t is the total diffusion constant. However, the Stokes-Einstein equation is not valid for anisotropic nanofibers (80% water fraction). Hence, the Stick hydrodynamic boundary condition was applied to modify the Stoke-Einstein equation (equation 4-6).[51, 66]

$$R_h = \frac{k_B T}{6\pi\eta D_t} \quad \ldots\ldots(3)$$

$$D_{\parallel} = \frac{k_B T}{2\pi\eta L} \ln\left(L/d\right) \quad \ldots\ldots(4)$$

$$D_{\perp} = \frac{k_B T}{4\pi\eta L} \ln\left(L/d\right) \quad \ldots\ldots(5)$$

$$D_t = (D_{\parallel} + 2D_{\perp})/3 \quad \ldots\ldots(6)$$

According to Stick's theory for rod-like particles, the diffusion coefficient parallel to the major axis ($D_{\parallel}$) is double that of the minor axis ($D_{\perp}$) (equation 6). L and d, are respectively the length and diameter of the rod. The equations 4-6 were solved by the Newton-Raphson method to calculate the length of the nanofibers.[51, 66] The results indicated the formation of ~ 2.05 μm average-sized nanofibers in the dispersion with 80% water content. Such smaller, elongated nanofibers formed in the dispersion could be further aggregated to provide a network of nanofibers upon solvent evaporation as revealed from the FESEM analysis of corresponding dried samples (Figure 2f). Thus, the FCS study, coupled with electron microscopy served as a guiding tool to unravel the morphological evolution of fluorescent aggregates in the aqueous

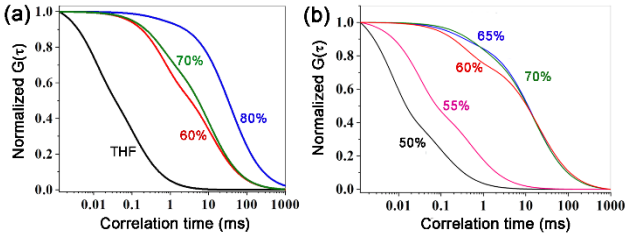

Figure 3. (a) Normalized FCS traces (λ_{ex} = 407 nm, λ_{em} = 435-800 nm) of TPAn solution (THF, 1 nM) and dispersion (2 μM, 3 mL) with varying the water fraction from 60% to 80% (the FCS data are fitted using equation 1, 2). (b) The discontinuity in the normalized FCS traces (50-70% water fraction) demonstrates the presence of both free and aggregated TPAn molecules (the FCS data were fitted using equation 1).

dispersion. At this juncture, we were curious to know the impact of the polarity of the microenvironment and the molecular structure on the self-assembly process.

Impact of solvent polarity. The gradual evolution of TPAn nanofibers in the THF-water mixture suggested that the self-assembly process was likely to be affected due to the change in the polarity of the medium. We further examined the aggregation of TPAn in the DMSO-water mixture to get a detailed insight. The abrupt spectral and morphological changes due to the aggregation were observed from 40% water fraction onwards. A steep rise in the plot of the extent of aggregation against the water fraction was also noticed at 30 to 40% water content. The most significant regime of aggregation of TPAn began at a much lesser content of water in a binary solvent mixture using DMSO than that of THF. The result was attributed to the higher polarity of DMSO over THF, indicating the effect of polarity on the self-assembly of TPAn. Additionally, the aggregation of TPAn in a solvent mixture of THF-hexane (hexane: nonpolar, aprotic, and bad solvent for TPAn) revealed no 1D morphological evolution, like in THF-water or DMSO-water.

Role of pyridinic nitrogen. The molecular structure along with the polarity of the medium plays a significant role in the formation of anisotropic nanoassembly.[1, 17] In the present case, the impact of pyridinic nitrogen centers of TPAn on the self-assembly process was verified through an acid-base-induced aggregation-deaggregation study. A reversible interconversion between the 1D-supramolecular nanofibers and nanoparticles was noticed with the addition of an equimolar amount of acid and base, respectively, into the dispersion of TPAn of 80% water fraction. The FESEM images revealed the gradual disaggregation of the pristine nanofibers to nanoparticles with time due to the protonation through the pyridinic nitrogen center upon the addition of acid (Figure 4a-d). The results were corroborated with the FCS study. The gradual disruption of nanofibers to solution-like dispersion with time in the presence of acid is shown in Figure 4h. Further, the emission peak of nanofibers at 630 nm successively decreased with a concomitant increase in the emission peak at 530 nm (solution like, Figure 4i). The reverse observations of the reformation of nanofibers from nanoparticles due to the addition of base into the acidified dispersion of TPAn were noticed through FESEM images

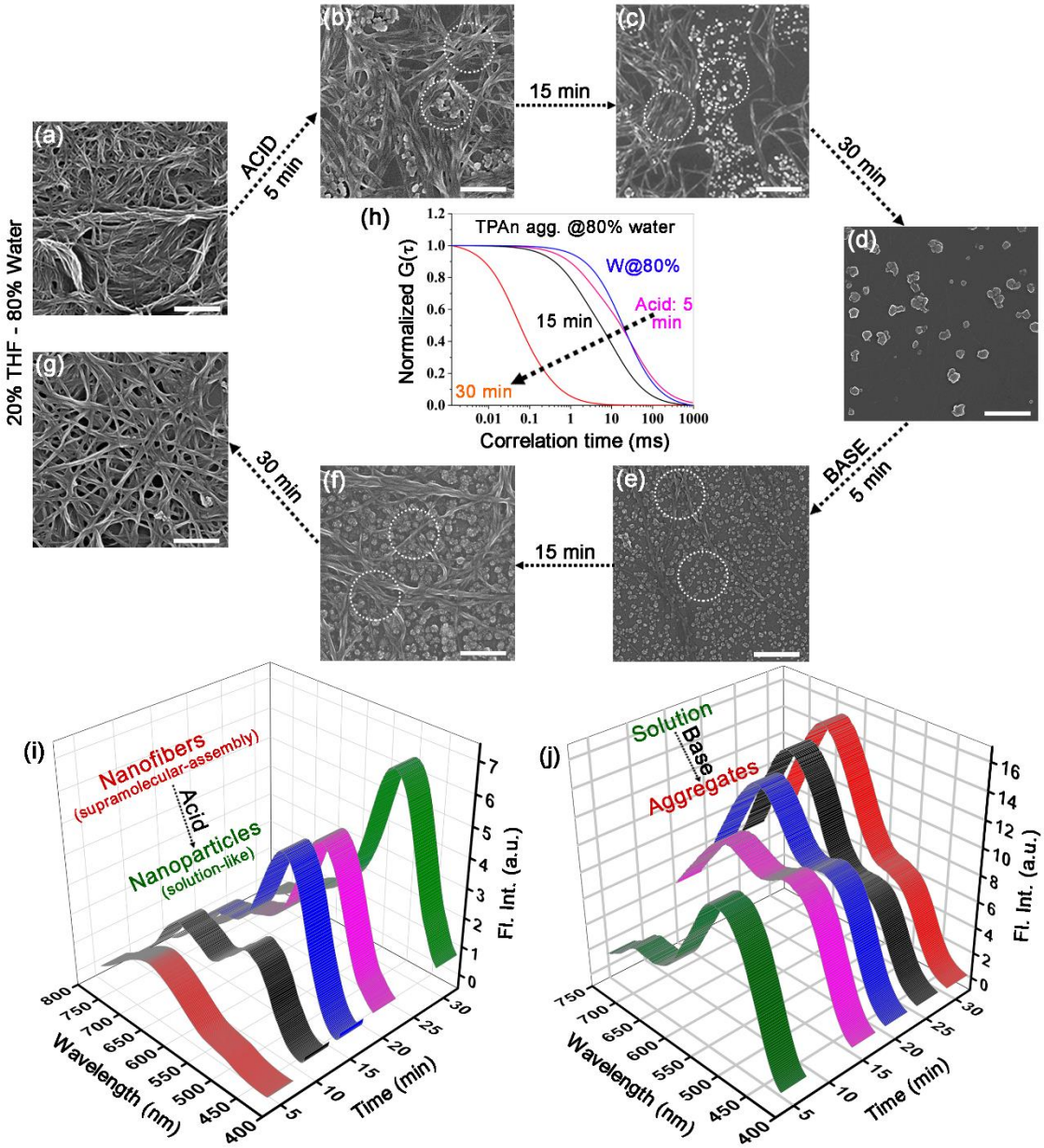

Figure 4. Acid-base-induced spontaneous self-assembly between 1D-supramolecular nanofibers and nanoparticles demonstrating the role of pyridinic nitrogen of TPAn [0.2 mM, 30 μL in 3 mL THF (20%) – water (80%) mixture]. FESEM images of (a) pristine nanofibers, (b-d) gradual disaggregation of nanofibers to nanoparticles with time upon addition of 50 μL, 1 mM HCl, and (e-g) successive reaggregation with time upon addition of 50 μL, 1 mM NaOH. (h) Normalized best fit FCS traces depicting disaggregation of TPAn nanofibers (80% water) to a solution-like signature with time upon addition of HCl. Steady-state emission spectra of TPAn dispersion (80% water fraction) upon addition of (i) acid (50 μL, 1 mM HCl) and (j) base (50 μL, 1 mM NaOH) on the resultant acidified dispersion demonstrating the gradual interconversion between 1D-supramolecular nanofibers and nanoparticles with time. Scale (Figure a-g) = 200 nm.

(Figure 4e-g). The results were further corroborated with emission spectra and FCS analysis (Figure 4j).

The FESEM and FCS analysis, coupled with steady-state emission measurements, revealed the definite impact of pyridinic nitrogen centers on the morphology of TPAn aggregates. Hence, we were intrigued by the nature of molecular packing and the noncovalent interactions governing the self-assembly of TPAn. The unit cell parameters of TPAn (orthorhombic, a = 14.6 Å, b = 12.5 Å, c = 6.9 Å, and $\alpha = \beta = \gamma = 90°$) were deduced through corroborating the experimental powder X-ray diffraction (PXRD) pattern with the Pawley refined profile using Materials Studio 6.1 package. Packing of TPAn molecules in the unit cells showed no intra- and intermolecular interactions. However, noncovalent interactions were noticed between the pyridinic 'N' center of one molecule and the CH hydrogens of the thiophene ring of another molecule (3.6 Å and 3.0 Å) in the adjacent unit cell when packed along the X-axis (Figure 5a). Similarly, the molecular packing along the Y-axis revealed the presence of intermolecular interactions between the 'N' center of the nitrile group and the CH hydrogens of the thiophene ring (3.8 Å and 2.9 Å) of two molecules in adjacent unit cells

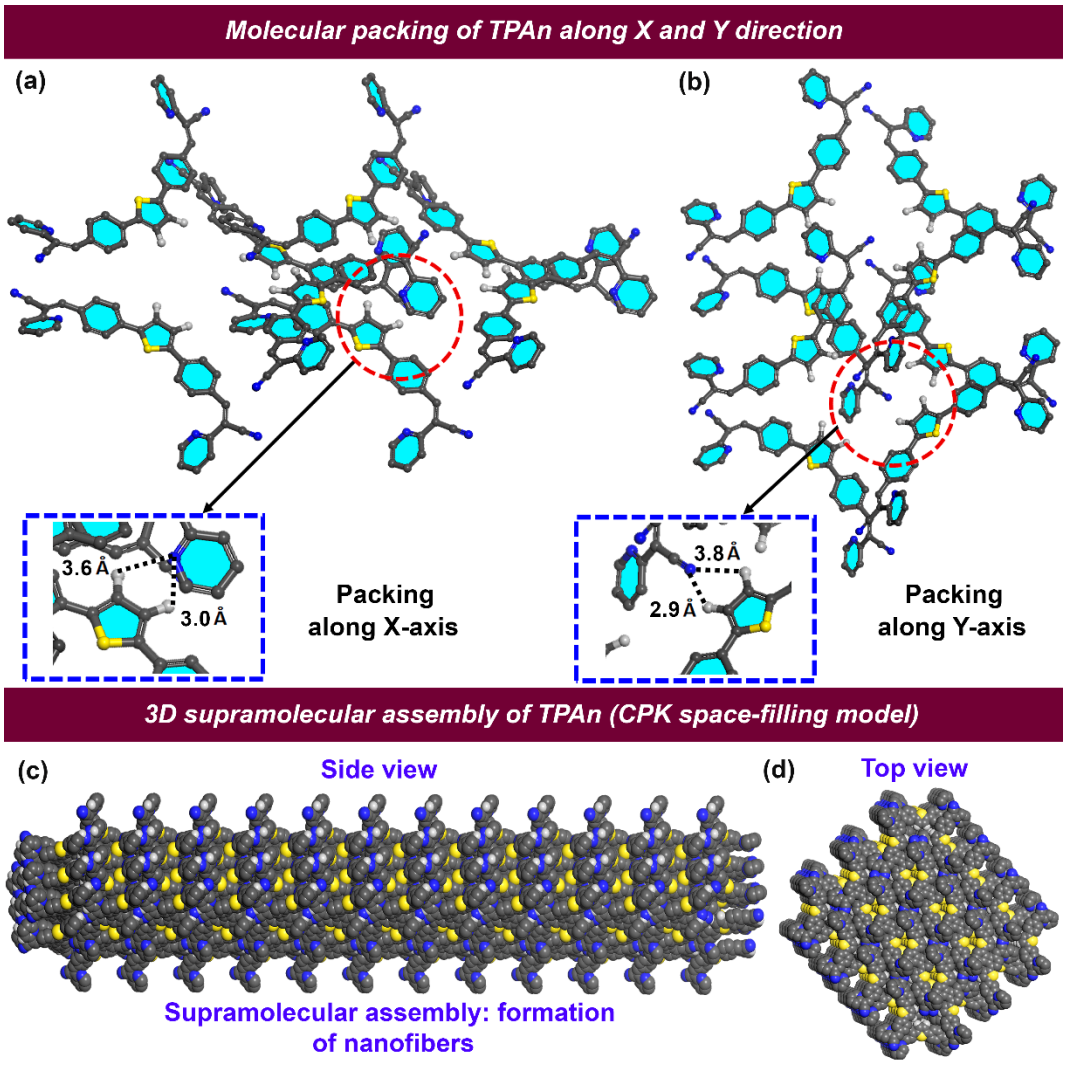

Figure 5. Molecular packing of TPAn in two adjacent unit cells showing the intermolecular interactions between (a) the pyridinic 'N' center of one molecule and the CH hydrogens of the thiophene ring of the other molecule (3.6 Å and 3.0 Å) along the X-axis, and (b) the 'N' center of nitrile group and the CH hydrogens of the thiophene ring of the adjacent molecule (3.8 Å and 2.9 Å) along the Y-axis. The unit cell was obtained through the Pawley refinement of powder X-ray diffraction pattern using the Materials Studio 6.1 package. The CPK (Corey-Pauling-Koltun) space-filling model of anisotropic self-assembled aggregates of TPAn: (c) side view, and (d) top view. Color code: C = grey, H = white, N = blue, and S = yellow; hydrogen atoms are omitted for clarity except those involved in noncovalent interactions.

(Figure 5b). Intermolecular interactions-driven three-dimensional (3D) supramolecular assembly suggested the formation of anisotropic architectures corroborating the results obtained through FESEM and FCS analysis (Figure 5c and 5d).

In addition to the computational investigations, a new compound without the pyridinic nitrogen centers (TPAnWN) was also synthesized (Figure 6a). A cuboid morphology was noticed in the FESEM and HRTEM images of the dispersion in THF-water mixture having the 80% fraction of water (Figure 6b). Furthermore, no change in the emission spectra was observed for TPAnWN aggregates upon the addition of acid (Figure 6c and 6d). The results unequivocally demonstrated the role of pyridinic 'nitrogen' centers in the formation of nanofibers at 80% fraction of hydrogen-bonding solvent water in THF. Inspired by the mechanistic exploration of supramolecular nanoaggregates formation by Würthner and coworkers,[44] we proposed a qualitative model demonstrating the evolution and growth of nanofibers from spherical nanoparticles considering spectroscopic results, microscopic observations, and molecular modeling analysis (Figure 7). The unique case of self-assembly leading to the morphological transformation of TPAn aggregates is governed by the molecular structure and the polarity of the medium.

Probing microenvironments. Since the fluorescence property of TPAn was sensitive to the local environments, we applied it to probe microenvironments inside a human cell. We anticipated that the hydrophobic TPAn might internalize to the lipid-enriched organelles, such as lipid droplets (LDs) through the hydrophobic interactions.[67, 68] The spectroscopic features of TPAn inside the living cells were probed through the fluorescence lifetime imaging (FLIM) using a time-resolved confocal microscope. A punctate dot-like pattern in the cytoplasm (λ_{ex} = 405 nm, λ_{em} = 435-800 nm),[69-72] and the colocalization images confirmed the internalization of TPAn in the lipid droplets. The diffusion time (τ_d) of TPAn in HeLa cells was

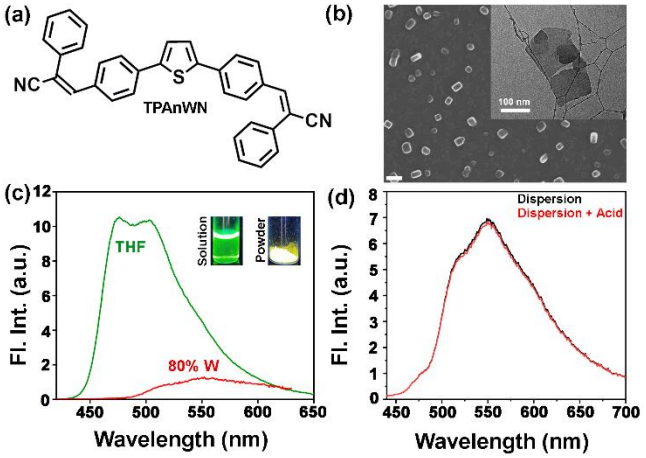

Figure 6. (a) Chemical structure of TPAnWN. (b) The FESEM image of TPAnWN aggregates in THF-water mixture with 80% water content illustrating a cuboid morphology. Inset: HRTEM image of TPAnWN aggregates. Scale = 100 nm. (c) Emission spectra (λ_{ex} = 410 nm) of TPAnWN in THF (5 μM) and TPAnWN (0.2 mM, 30 μL) in 3 mL THF-water mixture having the water fraction 80%; inset: the digital photographs showing green and yellowish-orange fluorescence of TPAnWN in the form of solution and powder, respectively under the illumination at 365 nm. (d) Emission spectra of TPAnWN dispersion (80% water fraction) before and after the addition of 50 μL, 1 mM HCl.

found to be 9 ms (Figure 8a), which is 90 times higher than that in THF. The results suggested the restriction of translational diffusion of TPAn after the internalization in LDs. The τ_d values of TPAn in LDs were comparable to that obtained in the aggregates (70% water content, Figure 8a). The diffusion time is inversely proportional to the viscosity of the medium. Hence, the viscosity sensed by TPAn in LDs was calculated and it was found to be 43 cP. The average lifetime (τ_{avg}) of TPAn in LDs (1.1 ns) was found to be in between solution and aggregates (Figure 8b). Even though the internalization of TPAn inside the cells occurred in the molecular form, the diffusion time and the fluorescence lifetime were increased similar to that observed in the

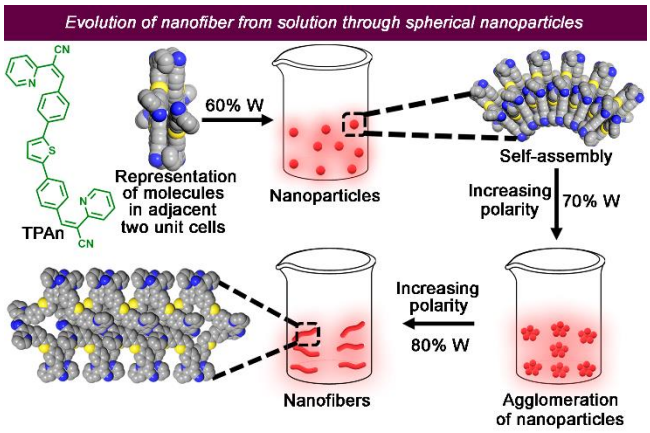

Figure 7. Schematic illustration depicting the morphological transformation of TPAn aggregates from spherical nanoparticles to anisotropic nanofibers. The supramolecular self-assembly leading to the formation of nanoparticles and nanofibers is represented using the CPK (Corey-Pauling-Koltun) space-filling model; unit cell of TPAn and the packing interactions are considered.

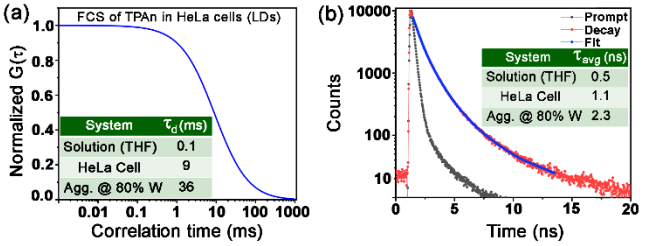

Figure 8. (a) FCS trace of TPAn inside the lipid droplets (LDs) in Hela cells; inset: diffusion time (τ_d) of TPAn in LDs as compared to that in solution and aggregated form. (b) Fluorescence lifetime decay profile of TPAn inside LDs in HeLa cells; inset: average lifetime (τ_{avg}) of TPAn in LDs compared to in solution and the aggregated form.

aggregates due to the specific localization in LDs through hydrophobic interactions. Thus, the systematic spectroscopic investigations unequivocally infer the critical role of hydrophobic-hydrophilic interactions for tuning the nature of self-assembly and the physical properties of a functional molecular optical material, TPAn, in the aqueous dispersion and inside the complex, heterogeneous medium, like human cells.

CONCLUSION

In conclusion, we rationalized the sequential molecular self-assembly pathways leading to intriguing morphological transformation from spherical nanoparticles to the network of nanofibers for a thiophene-based fluorescent probe (TPAn). The methodologies discussed in the present study are unique, providing a direct correlation between the morphology (solid-state characterization) and the emission properties (dispersion-state analysis). We performed a systematic investigation involving the steady-state absorption, emission, and FCS analysis coupled with FESEM and TEM. The electron microscopy results revealed the formation of the network of nanofibers for the dispersion having water content 80%. Whereas, FCS results implied the formation of smaller-sized nanofibers in the dispersion. Such nanofibers could be further agglomerated, leading to the formation of the network of nanofibers through solvent evaporation. The underlying mechanism of nanofiber formation was elucidated through examining (i) the nature of self-assembly in the THF-water, DMSO-water, THF-hexane mixture, (ii) the stimuli-responsive reversible morphological transformation of the aggregates, and (iii) molecular modeling studies. The results suggested that the polarity of the microenvironment and the presence of pyridinic nitrogen centers in TPAn governed the evolution of the nanofibers. Further, the optical properties of TPAn were compared in bulk solution, solid-state, molecular aggregates, and in the complex and heterogeneous medium, like HeLa cells. The general methodology developed in the current study paves the way to correlate the morphological evolution and optical properties of a diverse range of fluorescent aggregates through a combined microscopic and spectroscopic approach. Further expansion of the methodology may contribute toward a deeper understanding of the complex self-assembly processes in biological systems.

AUTHOR INFORMATION

Corresponding Authors

Abhijit Patra: *Department of Chemistry, Indian Institute of Science Education and Research Bhopal, Bhopal By-Pass Road, Bhauri, Bhopal 462066, Madhya Pradesh, India*; http://orcid.org/0000-0003-3144-1813;
Email: abhijit@iiserb.ac.in

Kankan Bhattacharyya: *Department of Chemistry, Indian Institute of Science Education and Research Bhopal, Bhopal By-Pass Road, Bhauri, Bhopal 462066, Madhya Pradesh;* http:// orcid.org/0000-0002-7463-3156;
Email: kankan@iiserb.ac.in

Authors

Subhankar Kundu: *Department of Chemistry, Indian Institute of Science Education and Research Bhopal, Bhopal By-Pass Road, Bhauri, Bhopal 462066, Madhya Pradesh, India*; http:// orcid.org/0000-0001-9294-5551; Email: subhankar16@iiserb.ac.in

Arkaprava Chowdhury: *Department of Chemistry, Indian Institute of Science Education and Research Bhopal, Bhopal By-Pass Road, Bhauri, Bhopal 462066, Madhya Pradesh, India*; http:// orcid.org/0000-0002-7582-9724; Email: arkapravachowdhury@gmail.com

Somen Nandi: *Department of Chemistry, Indian Institute of Science Education and Research Bhopal, Bhopal By-Pass Road, Bhauri, Bhopal 462066, Madhya Pradesh, India. Present address- Universitéde Bordeaux, Laboratoire Photonique Numérique et Nanosciences, UMR 5298, 33400 Talence, France and Institut d'Optique & CNRS, LP2N UMR 5298, 33400 Talence, France*. https://orcid.org/0000-0001-8484-761X; Email: somchemrnp@gmail.com

Notes

The authors declare no competing financial interest.

ACKNOWLEDGEMENTS

Financial support from BRNS, DAE (No. 37(2)/14/06/2016BRNS/37020), and the Council of Scientific and Industrial Research (CSIR), New Delhi (No. 01(2878)/17/EMR-II), infrastructural support from IISERB, and the FIST supported TEM facility to the Dept. of Chemistry, IISERB is gratefully acknowledged. K.B. thanks DST-SERB J C Bose National Fellowship. We thank Prof. Saptarshi Mukherjee for providing access to Spectrograph and acknowledge SERB (No. CRG/2018/000760) for funding the same. S.K. thanks UGC for the fellowship and Mr. Tapas Kumar Dutta for helping in molecular modelling studies.

REFERENCES

(1) Philp, D.; Stoddart, J. F. Self-Assembly in Natural and Unnatural Systems. *Angew. Chem. Int. Ed.* **1996**, *35*, 1154.
(2) Whitesides, G. M.; Grzybowski, B. Self-Assembly at All Scales. *Science* **2002**, *295*, 2418.
(3) Liu, Z.; Qiao, J.; Niu, Z.; Wang, Q. Natural Supramolecular Building Blocks: from Virus Coat Proteins to Viral Nanoparticles. *Chem. Soc. Rev*. **2012**, *41*, 6178.
(4) Nandi, N.; Bhattacharyya, K.; Bagchi, B. Dielectric Relaxation and Solvation Dynamics of Water in Complex Chemical and Biological Systems. *Chem. Rev.* **2000**, *100*, 2013.
(5) Ball, P. Water as an Active Constituent in Cell Biology. *Chem. Rev.* **2008**, *108*, 74.
(6) Mendes, A. C.; Baran, E. T.; Reis, R. L.; Azevedo, H. S. Self-Assembly in Nature: Using the Principles of Nature to Create Complex Nanobiomaterials. *Nanomed. Nanobiotech.* **2013**, *5*, 582.
(7) Bellissent, F. M. C.; Hassanali, A.; Havenith, M.; Henchman, R.; Pohl, P.; Sterpone, F.; van der Spoel, D.; Xu, Y.; Garcia, A. E. Water Determines the Structure and Dynamics of Proteins. *Chem. Rev.* **2016**, *116*, 7673.
(8) Breslow, R. Hydrophobic Effects on Simple Organic Reactions in Water. *Acc. Chem. Res.* **1991**, *24*, 159.
(9) Raschke, T. M.; Tsai, J.; Levitt, M. Quantification of the Hydrophobic Interaction by Simulations of the Aggregation of Small Hydrophobic Solutes in Water. *Proc. Nat. Acad. Sci.* **2001**, *98*, 5965.
(10) Chong, S. H.; Ham, S. Interaction with the Surrounding Water Plays a Key Role in Determining the Aggregation Propensity of Proteins. *Angew. Chem. Int. Ed.* **2014**, *53*, 3961.
(11) Jiang, L.; Cao, S.; Cheung, P. P. H.; Zheng, X.; Leung, C. W. T.; Peng, Q.; Shuai, Z.; Tang, B. Z.; Yao, S.; Huang, X. Real-time Monitoring of Hydrophobic Aggregation Reveals a Critical Role of Cooperativity in Hydrophobic Effect. *Nat. Commun.* **2017**, *8*, 15639.
(12) Oda, T.; Iwasa, M.; Aihara, T.; Maéda, Y.; Narita, A. The Nature of the Globular- to Fibrous-Actin Transition. *Nature* **2009**, *457*, 441.
(13) Madsen, M.; Gothelf, K. V. Chemistries for DNA Nanotechnology. *Chem. Rev.* **2019**, *119*, 6384.
(14) Lehn, J. M. Supramolecular Chemistry-Scope and Perspectives Molecules, Supermolecules, and Molecular devices. *Angew. Chem. Int. Ed.* **1988**, *27*, 89.
(15) Fresnais, J.; Ishow, E.; Sandre, O.; Berret, J. F. Electrostatic Co-Assembly of Magnetic Nanoparticles and Fluorescent Nanospheres: A Versatile Approach Towards Bimodal Nanorods. *Small* **2009**, *5*, 2533.
(16) Chakrabarty, R.; Mukherjee, P. S.; Stang, P. J. Supramolecular Coordination: Self-Assembly of Finite Two- and Three-Dimensional Ensembles. *Chem. Rev.* **2011**, *111*, 6810.
(17) Stupp, S. I.; Palmer, L. C. Supramolecular Chemistry and Self-assembly in Organic Materials Design. *Chem. Mater.* **2014**, *26*, 507.
(18) Kim, J.; Baek, K.; Shetty, D.; Selvapalam, N.; Yun, G.; Kim, N. H.; Ko, Y. H.; Park, K. M.; Hwang, I.; Kim, K. Reversible Morphological Transformation Between Polymer Nanocapsules and Thin Films Through Dynamic Covalent Self-Assembly. *Angew. Chem. Int. Ed.* **2015**, *54*, 2693.
(19) Zou, R.; Wang, Q.; Wu, J.; Wu, J.; Schmuck, C.; Tian, H. Peptide Self-Assembly Triggered by Metal Ions. *Chem. Soc. Rev.* **2015**, *44*, 5200.
(20) Wu, G.; Chen, S. C.; Liu, C. L.; Wang, Y. Z. Direct Aqueous Self-Assembly of an Amphiphilic Diblock Copolymer Toward Multistimuli-Responsive Fluorescent Anisotropic Micelles. *ACS Nano.* **2015**, *9*, 4649.
(21) Ji, X.; Wang, H.; Li, Y.; Xia, D.; Li, H.; Tang, G.; Sessler, J. L.; Huang, F. Controlling Amphiphilic Copolymer Self-Assembly Morphologies Based on Macrocycle/Anion Recognition and Nucleotide-Induced Payload Release. *Chem. Sci.* **2016**, *7*, 6006.
(22) Hendricks, M. P.; Sato, K.; Palmer, L. C.; Stupp, S. I. Supramolecular Assembly of Peptide Amphiphiles. *Acc. Chem. Res.* **2017**, *50*, 2440.
(23) Mittal, N.; Jansson, R.; Widhe, M.; Benselfelt, T.; Håkansson, K. M. O.; Lundell, F.; Hedhammar, M.; Söderberg, L. D. Ultrastrong and Bioactive Nanostructured Biobased Composites. *ACS Nano* **2017**, *11*, 5148.
(24) Syamala, P. P. N.; Soberats, B.; Görl, D.; Gekle, S.; Würthner, F. Thermodynamic Insights into the Entropically Driven Self-Assembly of Amphiphilic Dyes in Water. *Chem. Sci.* **2019**, *10*, 9358.

(25) Dong, M.; Wessels, M. G.; Lee, J. Y.; Su, L.; Wang, H.; Letteri, R. A.; Song, Y.; Lin, Y. N.; Chen, Y.; Li, R.; Pochan, D. J.; Jayaraman, A.; Wooley, K. L. Experiments and Simulations of Complex Sugar-Based Coil–Brush Block Polymer Nanoassemblies in Aqueous Solution. *ACS Nano.* **2019**, *13*, 5147.
(26) Ochs, N. A. K.; Lewandowska, U.; Zajaczkowski, W.; Corra, S.; Reger, S.; Herdlitschka, A.; Schmid, S.; Pisula, W.; Müllen, K.; Bäuerle, P.; Wennemers, H. Oligoprolines Guide the Self-Assembly of Quaterthiophenes. *Chem. Sci.* **2019**, *10*, 5391.
(27) Xiong, R.; Yu, S.; Smith, M. J.; Zhou, J.; Krecker, M.; Zhang, L.; Nepal, D.; Bunning, T. J.; Tsukruk, V. V. Self-Assembly of Emissive Nanocellulose/ Quantum Dot Nanostructures for Chiral Fluorescent Materials. *ACS Nano.* **2019**, *13*, 9074.
(28) Ajayaghosh, A.; George, S. J. First Phenylenevinylene Based Organogels: Self-Assembled Nanostructures via Cooperative Hydrogen Bonding and π-Stacking. *J. Am. Chem. Soc.* **2001**, *123*, 5148.
(29) An, B. K.; Lee, D. S.; Lee, J. S.; Park, Y. S.; Song, H. S.; Park, S. Y. Strongly fluorescent organogel system comprising fibrillar self-assembly of a trifluoromethyl-based cyanostilbene derivative. *J. Am. Chem. Soc.* **2004**, *126*, 10232.
(30) Yamamoto, T.; Fukushima, T.; Yamamoto, Y.; Kosaka, A.; Jin, W.; Ishii, N.; Aida, T. Stabilization of a Kinetically Favored Nanostructure: Surface ROMP of Self-Assembled Conductive Nanocoils from a Norbornene-Appended Hexa-Peri-Hexabenzocoronene. *J. Am. Chem. Soc.* **2006**, *128*, 14337.
(31) Palmer, L. C.; Stupp, S. I. Molecular Self-Assembly into One-Dimensional Nanostructures. *Acc. Chem. Res.* **2008**, *41*, 1674.
(32) Kim, H. J.; Kim, T.; Lee, M. Responsive Nanostructures From Aqueous Assembly of Rigid-Flexible Block Molecules. *Acc. Chem. Res.* **2011**, *44*, 72.
(33) An, B. K.; Gierschner, J.; Park, S. Y. π-Conjugated Cyanostilbene Derivatives: A Unique Self-Assembly Motif for Molecular Nanostructures with Enhanced Emission and Transport. *Acc. Chem. Res.* **2012**, *45*, 544.
(34) Chi, X.; Zhang, H.; Vargas-Zúñiga, G. I.; Peters, G. M.; Sessler, J. L. A Dual-Responsive Bola-Type Supra-Amphiphile Constructed from a Water-Soluble Calix[4]Pyrrole and a Tetraphenylethene-Containing Pyridine Bis-*N*-oxide. *J. Am. Chem. Soc.* **2016**, *138*, 5829.
(35) Grande, V.; Soberats, B.; Herbst, S.; Stepanenko, V.; Würthner, F. Hydrogen-Bonded Perylene Bisimide J-Aggregate Aqua Material. *Chem. Sci.* **2018**, *9*, 6904.
(36) Xing, P.; Zhao, Y. Multifunctional Nanoparticles Self-Assembled from Small Organic Building Blocks for Biomedicine. *Adv. Mater.* **2016**, *28*, 7304.
(37) Wang, Q.; Li, Z.; Tao, D. D.; Zhang, Q.; Zhang, P.; Guo, D. P.; Jiang, Y. B. Supramolecular Aggregates as Sensory Ensembles. *Chem. Commun.* **2016**, *52*, 12929.
(38) Kumar, V.; Sk, B.; Kundu, S.; Patra, A. Dynamic and Static Excimer: a Versatile Platform for Single Component White-Light Emission and Chelation-Enhanced Fluorescence. *J. Mater. Chem. C.* **2018**, *6*, 12086.
(39) Pallavi, P.; Kumar, V.; Hussain, M. D. W.; Patra, A. Excited-State Intramolecular Proton Transfer-Based Multifunctional Solid-State Emitter: A Fluorescent Platform with "Write-Erase-Write" Function. *ACS Appl. Mater. Interfaces* **2018**, *10*, 44696.
(40) Cheng, H. B.; Li, Y.; Tang, B. Z.; Yoon, J. Assembly Strategies of Organic-Based Imaging Agents for Fluorescence and Photoacoustic Bioimaging Applications. *Chem. Soc. Rev.* **2020**, *49*, 21.
(41) Kundu, S.; Sk, B.; Pallavi, P.; Giri, A.; Patra, A. Molecular Engineering Approaches Towards All-Organic White Light Emitting Materials. *Chem. Eur. J.* **2020**, *26*, 5557.
(42) Fu, H. B.; Yao, J. N. Size Effects on the Optical Properties of Organic Nanoparticles. *J. Am. Chem. Soc.* **2001**, *123*, 1434.
(43) Patra, A.; Hebalkar, N.; Sreedhar, B.; Sarkar, M.; Samanta, A.; Radhakrishnan, T. P. Tuning the Size and Optical Properties in Molecular Nano/ Microcrystals: Manifestation of Hierarchical Interactions. *Small* **2006**, *2*, 650.
(44) Zhang, X.; Chen, Z.; Würthner, F. Morphology Control of Fluorescent Nanoaggregates by Co-Self-Assembly of Wedge- and Dumbbell-shaped Amphiphilic Perylene Bisimides. *J. Am. Chem. Soc.* **2007**, *129*, 4886.
(45) O'Brien, E. P.; Straub, J. E.; Brooks, B. R.; Thirumalai, D. Influence of Nanoparticle Size and Shape on Oligomer Formation of an Amyloidogenic Peptide. *J. Phys. Chem. Lett.* **2011**, *2*, 1171.
(46) Higashiguchi, K.; Taira, G.; Kitai, J. I.; Hirose, T.; Matsuda, K. Photoinduced Macroscopic Morphological Transformation of an Amphiphilic Diarylethene Assembly: Reversible Dynamic Motion. *J. Am. Chem. Soc.* **2015**, *137*, 2722.
(47) Chen, Z.; Fimmel, B.; Würthner, F. Solvent and Substituent Effects on Aggregation Constants of Perylene Bisimide π-Stacks–a Linear Free Energy Relationship Analysis. *Org. Biomol. Chem.* **2012**, *10*, 5845.
(48) Jin, Q.; Zhang, L.; Liu, M. Solvent-Polarity-Tuned Morphology and Inversion of Supramolecular Chirality in a Self-Assembled Pyridylpyrazole-Linked Glutamide Derivative: Nanofibers, Nanotwists, Nanotubes, and Nicrotubes. *Chem. Eur. J.* **2013**, *19*, 9234.
(49) Maity, A.; Gangopadhyay, M.; Basu, A.; Aute, S.; Babu, S. S.; Das, A. Counteranion Driven Homochiral Assembly of a Cationic C_3-Symmetric Gelator through Ion-Pair Assisted Hydrogen Bond. *J. Am. Chem. Soc.* **2016**, *138*, 11113.
(50) Yang, S.; Choi, T. L. Rapid Formation and Real-Time Observation of Micron-Sized Conjugated Nanofibers with Tunable Lengths and Widths in 20 Minutes by Living Crystallization-Driven Self-Assembly. *Chem. Sci.* **2020**, *11*, 8416.
(51) Sharma, S.; Pal, N.; Chowdhury, P. K.; Sen, S.; Ganguli, A. K. Understanding Growth Kinetics of Nanorods in Microemulsion: A Combined Fluorescence Correlation Spectroscopy, Dynamic Light Scattering, and Electron Microscopy Study. *J. Am. Chem. Soc.* **2012**, *134*, 19677.
(52) Schaeffel, D.; Staff, R. H.; Butt, H. J.; Landfester, K.; Crespy, D.; Koynov, K. Fluorescence Correlation Spectroscopy Directly Monitors Coalescence During Nanoparticle Preparation. *Nano Lett.* **2012**, *12*, 6012.
(53) Blokzijl, W.; Engberts, J. B. F. N. Hydrophobic Effects. Opinions and Facts. *Angew. Chem. Int. Ed.* **1993**, *32*, 1545.
(54) Davies, T. S.; Ketner, A. M.; Raghavan, S. R. Self-Assembly of Surfactant Vesicles that Transform into Viscoelastic Wormlike Micelles upon Heating. *J. Am. Chem. Soc.* **2006**, *128*, 6669.
(55) Cai, Y.; Guo, Z.; Chen, J.; Li, W.; Zhong, L.; Gao, Y.; Jiang, L.; Chi, L.; Tian, H.; Zhu, W. H. Enabling Light Work in Helical Self-Assembly for Dynamic Amplification of Chirality with Photoreversibility. *J. Am. Chem. Soc.* **2016**, *138*, 2219.
(56) Li, R.; Wang, H.; Song, Y.; Lin, Y.-N.; Dong, M.; Shen, Y.; Khan, S.; Zhang, S.; Fan, J.; Zhang, F.; Su, L.; Wooley, K. L. In Situ Production of Ag/polymer Asymmetric Nanoparticles via a Powerful Light-Driven Technique. *J. Am. Chem. Soc.* **2019**, *141*, 19542.
(57) Gomar-Nadal, E.; Puigmartí-Luis, J.; Amabilino, D. B. Assembly of Functional Molecular Nanostructures on Surfaces. *Chem. Soc. Rev.* **2008**, *37*, 490.
(58) Bishop, K. J. M.; Wilmer, C. E.; Soh, S.; Grzybowski, B. A. Nanoscale Forces and Their Uses in Self-assembly. *Small* **2009**, *5*, 1600.
(59) Deng, K.; Luo, Z.; Tan, L.; Quan, Z. Self-Assembly of Anisotropic Nanoparticles into Functional Superstructures. *Chem. Soc. Rev.* **2020**, *49*, 6002.
(60) Mukherjee, S.; Kim, K.; Nair, S. Short, Highly Ordered, Single-Walled Mixed-Oxide Nanotubes Assemble from Amorphous Nanoparticles. *J. Am. Chem. Soc.* **2007**, *129*, 6820.
(61) Singh, J.; Sabareesan, A. T.; Mathew, M. K.; Udgaonkar, J. B. Development of the Structural Core and of Conformational Heterogeneity during the Conversion of Oligomers of the Mouse Prion Protein to Worm-like Amyloid Fibrils. *J. Mol. Bio.* **2012**, *423*, 217.
(62) Lakowicz, J. R. Principles of Fluorescence Spectroscopy. *Springer*, New York, **2006**.

(63) Garai, K.; Sahoo, B.; Kaushalya, S. K.; Desai, R.; Maiti, S. Zinc Lowers Amyloid-β Toxicity by Selectively Precipitating Aggregation Intermediates. *Biochemistry* **2007**, *46*, 10655.
(64) Winkler, P. M.; Regmi, R.; Flauraud, V.; Brugger, J.; Rigneault, H.; Wenger, J.; García-Parajo, M. F. **O**ptical Antenna-Based Fluorescence Correlation Spectroscopy to Probe the Nanoscale Dynamics of Biological Membranes. *J. Phys. Chem. Lett.* **2018**, *9*, 110.
(65) Dong, C.; Irudayaraj, J. Hydrodynamic Size-Dependent Cellular Uptake of Aqueous QDs Probed by Fluorescence Correlation Spectroscopy. *J. Phys. Chem. B* **2012**, *116*, 12125.
(66) Vasanthi, R.; Ravichandran, S.; Bagchi, B. Needlelike Motion of Prolate Ellipsoids in the Sea of Spheres. *J. Chem. Phys.* **2001**, *114*, 7989.
(67) Ghosh, S.; Chattoraj, S.; Mondal, T.; Bhattacharyya, K. Dynamics in Cytoplasm, Nucleus, and Lipid Droplet of a Live CHO Cell: Time-Resolved Confocal Microscopy. *Langmuir* **2013**, *29*, 7975.
(68) Sk, B.; Thakre, P. K.; Tomar, R. S.; Patra, A. A Pyridoindole-Based Multifunctional Bioprobe: pH-Induced Fluorescence Switching and Specific Targeting of Lipid Droplets. *Chem. Asian J.* **2017**, *12*, 2501.
(69) Nandi, S.; Ghosh, S.; Bhattacharyya, K. Live Cell Microscopy: A Physical Chemistry Approach. *J. Phys. Chem. B* **2018**, *122*, 3023.
(70) Olzmann, J. A.; Carvalho, P. Dynamics and Functions of Lipid Droplets. *Nat. Rev. Mol. Cell Biol.* **2019**, *20*, 137.
(71) Zheng, X.; Zhu, W.; Ni, F.; Ai, H.; Gong, S.; Zhou, X.; Sessler, Jonathan L.; Yang, C. Simultaneous Dual-Colour Tracking Lipid Droplets and Lysosomes Dynamics Using a Fluorescent Probe. *Chem. Sci.* **2019**, *10*, 2342.
(72) Collot, M.; Bou, S.; Fam, T. K.; Richert, L.; Mély, Y.; Danglot, L.; Klymchenko, A. S. Probing Polarity and Heterogeneity of Lipid Droplets in Live Cells Using a Push–Pull Fluorophore. *Anal. Chem.* **2019**, *91*, 1928.